ACADEMIC PRESS

Available online at www.sciencedirect.com
SCIENCE DIRECT®

NeuroImage

NeuroImage 20 (2003) 1765–1774

www.elsevier.com/locate/ynimg

Is the brain cortex a fractal?

Valerij G. Kiselev,[a,*] Klaus R. Hahn,[b] and Dorothee P. Auer[c]

[a] *Institute of Medicine, Research Center Jülich, GmBH, D-52425 Jülich, Germany*
[b] *Institute of Biomathematics and Biometry, GSF, Research Center for Environment and Health, Oberschleissheim, Germany*
[c] *Max Plank Institute of Psychiatry, NMR Research Group, Munich, Germany*

Received 23 October 2002; revised 10 June 2003; accepted 23 June 2003

Abstract

The notion of fractal has been largely used to describe geometrical properties of complex objects in biology and medicine. In the present study the question is addressed whether the human cerebral cortex is self-similar in a statistical sense, which is commonly referred to as being a fractal. A new calculational method is presented, which is volumetric and based on the fast Fourier transform (FFT) of segmented three-dimensional high-resolution magnetic resonance images. The analysis covers a wide range of spatial scales from the size of the whole cortex to the ultimate pixel size. Results obtained in six subjects confirm the fractal nature of the human cerebral cortex down to a spatial scale of 3 mm. The obtained fractal dimension is $D = 2.80 \pm 0.05$, which is in reasonable agreement with previously reported results. Deployment of FFT enables a simple interpretation of the results and yields a high performance, which is necessary to analyze the entire cortex. Thus the FFT-based analysis of segmented MR images offers a comprehensive approach to study neurodevelopmental and neurodegenerative changes in the fractal geometry of the cerebral cortex.

1. Introduction

The complexity of the human cerebral cortex geometry suggests a description based on the notion of a fractal, a mathematical construction dedicated to describe the self-similarity of various objects in dead and living nature (see, e.g., Liu, 1986; Cook et al., 1995; a brief introduction into the notion of fractal is given below). The fundamental question to be answered is whether the cortex is indeed self-similar. This would mean that the statistical properties of the gyral pattern of small cortex structures are similar to those of large ones. This approach refers to averaged characteristics of the brain in contrast to the precise anatomic description of individual structures. If the human cerebral cortex will be shown to be a fractal structure, then geometrical abnormalities of the overall gyral pattern, which is difficult to assess by standard morphometric tools, may be studied by fractal analysis.

The present problem has its own history. Hofman (1991) gave a strong argument in favor of the fractal geometry of the human cortex based on a surface-to-volume relation in the mammalian brains. Majumdar and Prasad (1988) found a fractal dimension $D = 2.60 \pm 0.5$ for the external cortex surface in normal subjects using magnetic resonance (MR) images of brain sections. The performed analysis was based on the box counting method, which provided a measure for the length of cortical interface in each slice. The result was extrapolated to three dimensions by adding unity, which is a correct procedure for isotropic fractals. A three-dimensional analysis of a fixed brain specimen was performed by Chuang et al. (1991) with the result $D = 2.20$. They applied the surface tracking, which is a generalization of the box counting method for three dimensions. Both studies were criticized by Free et al. (1996) for giving little information about details of MR imaging and data processing. Free et al. investigated the interface between the human white and gray matter obtained from segmented volumetric MR data. They found that smoothing of the reconstructed white matter surface reduces its area in agreement with the hypothesis of fractal geometry and reported a fractal dimension $D = 2.30 \pm 0.01$. Note that this fractal dimension was obtained

* Corresponding author. Present address: Section of Medical Physics, Department of Diagnostic Radiology, University Hospital Freiburg, Hugstetterstr. 55, D-79102 Freiburg, Germany. Fax: +49-761-2703831.
E-mail address: kiselev@ukl.uni-freiburg.de (V.G. Kiselev).

1053-8119/$ – see front matter © 2003 Elsevier Inc. All rights reserved.
doi:10.1016/S1053-8119(03)00380-X

from five smoothing levels ranging from 1.4 to 6.1 mm with interpolation of the original voxel size to $0.47 \times 0.47 \times 0.36$ mm^3. While this study provides support for the hypothesis that the white matter surface is fractal, the small amount of smoothing levels does not allow to draw conclusions about its entire geometry.

Cook et al. (1995) showed that the cortex reveals basically similar patterns of folds and islands up to a magnification of about 14 times the original. They studied MR slices by the box counting method in the scale range 25–2.5 mm and found a fractal dimension 1.45 ± 0.06 for the gray–white matter interface using seven smoothing levels. Moreover, a reduced fractal dimension of $D < 1.27$ was found in about half of the studied patients with frontal lobe epilepsy. This is in line with a previous report of this group by Free et al. (1996) showing abnormal fractal dimensions in about half of the patients with epilepsy.

The complexity of the cortex folding, which is characterized by the fractal dimension, increases with the normal brain development as studied over the first two decades of life by Blanton et al. (2001) in normal children. The value was close to 2.26 and varied between lobes with the most pronounced age-dependant increase in the left superior and inferior frontal gyri. The method was based on MR imaging accompanied by the surface smoothing method developed by Thompson et al. (1996) to analyze the cortical geometry using brain sections. The latter study resulted in the fractal dimension in the range 2.09–2.12 depending on the cortical structure studied.

These studies indicate the potential of quantifying the complexity of the cortical folding for further characterization of normal and abnormal brain development including mental and neurological diseases such as schizophrenia and epilepsy.

The use of the fractal dimension as a measure for the cortical complexity relies on the assumption of self-similarity of the cortex. In all studies except of one performed by Majumdar and Prasad (1988) this hypothesis has been verified only for restricted spatial scales. In this article we propose a novel computational method and analyze the entire geometry of the human cerebral cortex. The range of spatial scales over which the cortex is self-similar and the respective fractal dimensions are shown. This is enabled by the use of the fast Fourier transform, well suited to fast three-dimensional automated geometry analysis over the whole range of spatial scales.

2. Materials and methods

2.1. Brief introduction to fractal geometry

Let us briefly review the properties of fractals which are essential for the present study. A more detailed introduction in the context of cortical folding was offered by Cook et al. (1995) The notion of dimensionality stems from everyday experience. For example, a thin wire is one- and a sheet of paper is two-dimensional. A mathematical definition, which digests this common sense, can be formulated as follows. Consider an object, the dimension of which is to be determined. One has to take an element of this object. The element may be, for example, a voxel or a molecule. One has to surround it with a sphere of a given radius R and count the amount of object elements, υ, inside the sphere. The measure of υ can be arbitrary; it can be, for example, the amount of voxels or the volume. Of importance is only the dependence of υ on the sphere radius after averaging over the element put in its origin. This value scales as $\upsilon \propto R^D$ where D is the dimension by definition. This definition not only meets the everyday experience for the simplest cases mentioned above, but also takes into account the fact that the relevant dimension of an object depends on the spatial scale. For example, both the wire and the paper sheet show the dimension of three at short distances for which the sphere radius, R, is smaller than their thickness. At higher R a transition to the dimensions of one or two occurs. Thus even the simplest examples instructively highlight the importance of crossovers in the dependence of the dimension on the spatial scale, R. These change points indicate the characteristic lengths which are present in the investigated object.

The above definition can be reformulated in order to become a practical mathematical tool. Consider an object in three-dimensional space. The average amount of matter, υ, in a sphere of radius R is equal to

$$\upsilon(R) = \int_{r<R} \rho(\mathbf{r}) d^3\mathbf{r}, \tag{1}$$

where $\rho(\mathbf{r})$ is the probability to find two object elements at the separation $\mathbf{r}$. The integration is performed over the sphere volume with r denoting the absolute value of vector $\mathbf{r}$: $r = |\mathbf{r}|$. Function $\rho(\mathbf{r})$ provides a detailed description of the geometry of the considered object. This function is known under different names in many physical contexts. Here we refer to it as the density–density correlation function, $\rho(\mathbf{r})$, the name is borrowed from condensed matter physics.

Consider objects, which are isotropic in a statistical sense. This implies in particular that the function $\rho(\mathbf{r})$ does not depend on the direction of vector $\mathbf{r}$. The above definition of the fractal dimension accounting for Eq. (1) requires ρ to depend on a power of r:

$$\rho(\mathbf{r}) = \text{Const} \cdot r^{D-3}. \tag{2}$$

Self-similarity is the second issue involved in the present analysis. It implies that the object looks similar to its zoomed part. The words “looks similar” demand a proper mathematical definition. As such, one requires that the averaged object density, which is obtainable from $\upsilon(R)$, and the density–density correlation functions derived from the main and the zoomed images have the same form. In view

of Eq. (2) this means an invariance of the object dimension D with respect to zooming. This requirement defines the self-similarity in the wide sense. In contrast, the strict-sense self-similarity implies the conservation of all statistical properties upon zooming. This property can hardly be verified in biological objects imaged with a finite resolution. The self-similarity discussed hereafter is understood in the wide sense.

The fractals are nontrivial self-similar objects. The trivial ones are, for example, a straight line, a plane, or three-dimensional space. The dimension D for fractals takes fractional values, which has originated the name. For any fractal object, which exists in nature, it is possible to find a range of spatial scales over which the fractal geometry holds. For example, the coast line remains a fractal over the lengths from the island size to that of a single rock. In the present study special attention is paid to inspecting the self-similarity range of the human cerebral cortex.

2.2. Analysis of cortex geometry

The presented method refers to the density–density correlation function $\rho(\mathbf{r})$, which, for the case of the cerebral cortex is the probability to find two voxels in the cortex separated by a given vector $\mathbf{r}$. In fractals this function scales according to Eq. (2) as r^{D-3}, where $r = |\mathbf{r}|$ and D is the fractal dimension. This dependence yields a straight line when plotted in the double logarithmic scale. The reported method is applied to segmented brain images (obtained as described below), in which the cortical gray matter is assigned a value of unity, while the brightness of all other voxels is set to zero. Mathematically such an image can be described as a function of voxel position, $\mathbf{r}$. This function will be refered to as the cortical shape function and will be denoted as $s(\mathbf{r})$.

In principle, calculation of $\rho(\mathbf{r})$ is possible via a straightforward voxel counting in the segmented brain images. However, this procedure results in a huge number of operations of the order of N^2, where N is the total number of voxels. For high-resolution anatomical MR images as those used in the present study $N \approx 2^{26}$ and data processing becomes extremely time-consuming. A similar problem is inherent in the previous approaches based on measuring the cortical area (Cook et al., 1995; Free et al., 1996; Thompson et al., 1996).

We solve this problem by working with the Fourier transform, $f(\mathbf{k})$, of the shape function, $s(\mathbf{r})$, of the segmented cortex from which we recollect the necessary information about the correlation function $\rho(\mathbf{r})$. The use of the fast Fourier transform reduces the huge amount of computations, since it requires only about $N \ln N$ operations. The gain in performance for the high-resolution anatomical images is two orders of magnitude.

For the analysis, the squared magnitude $|f(\mathbf{k})|^2$ is averaged over the directions of the wave vector $\mathbf{k}$. This yields a function $F(k)$ which is real and depends only on the absolute value $k = |\mathbf{k}|$,

$$F(k) = \frac{1}{4\pi}\int_0^{2\pi} d\varphi \int_0^{\pi} d\theta \sin\theta \, |f(\mathbf{k})|^2, \tag{3}$$

where φ and θ are the polar and the azimuthal angles that define the direction of vector $\mathbf{k}$.

As shown in the Appendix, $F \propto k^{-D}$ for fractals. Thus a straight segment in the double logarithmic plot of $F(k)$ indicates a self-similarity range of the cortex. There might be several straight sections with different values of D. The cross-overs between them indicate scales at which the cortex geometry changes.

2.3. MR brain imaging

Magnetic resonance images were obtained at 1.5 T (Signa Echospeed, GE Medical Systems, Milwaukee, WI). High-resolution, whole-brain T1-weighted spoiled gradient echo data sets (SPGR, IR-PREPPED, repetition time (TR) = 10.3 ms, echo time (TE) = 3.4 ms, field of view (FOV) = 23×23 cm^2, matrix size = 256×256, flip angle = 20°) were acquired in the sagittal plane with an in-plane resolution of 0.90×0.90 mm^2. The three-dimensional data sets consisted of 128 contiguous slices of thickness 1.4 mm. Six subjects were included in this study, consisting of four young healthy male volunteers (Subjects 2–5, age range 21 to 30 years), a middle-aged healthy man (Subject 1, 56 years), and a women with focal cortical malformation (Subject 6, 55 years).

2.4. Image segmentation

The gray matter was segmented from the measured data by a method which was published in preliminary versions in several proceedings (Hahn et al., 2000, 2001a, 2001b); an essentially improved variant is applied in the present work. The corresponding preprint can be delivered on request. This nonparametric intensity segmentation method eliminates after skull pealing via several correction steps distortion and noise artifacts. Finally, after nonlinear edge preserving noise elimination global thresholds are introduced to separate CSF, and gray and white matter. No shape prior is used, so the method applies equally well to normal and malformed brains. The main new features are axial and irregular bias corrections which are based on an estimate of the cortex distortions in contrast to the frequently used white matter-based corrections with subsequent extrapolation to the cortex, see, e.g., Dale et al. (1999). The non-equivalence of gray or white matter-based distortion fields is one of the interesting outcomes of this segmentation study (Hahn et al., 2001a, 2001b). This method is especially well suited to the present fractal analysis, as the considered measure is derived from volumetric cortex properties and as

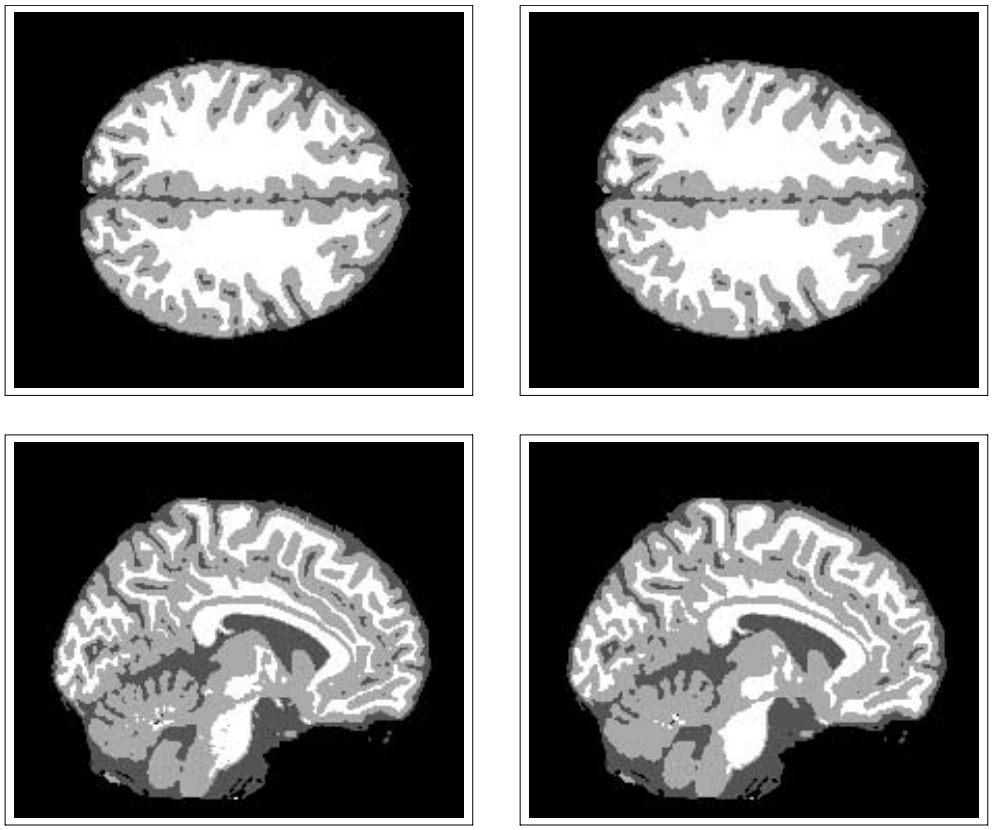

Fig. 1. CSF, and gray and white matter of an axial and a sagittal slice in obvious coloring. Left panels show the labeling of the Montreal brain phantom, right panels the thresholded result of the segmentation method applied to the phantom with a 3% noise level and with 40% RF nonuniformity.

the cortex distortions are removed with higher precision than those in white matter. The method requires few user interactions to control the parameter settings; by renunciation of a perfect automation it gains flexibility and precision. To test precision, the Montreal brain phantom (Kwan et al., 1996; Cocosco et al., 1997) was segmented for a noise level of 3% and a distortion of 40% RF nonuniformity, which roughly approximates the distortions in our real data. A quantitative measure of the segmentation quality is given by the κ statistics (Ashburner and Friston, 2000), measuring the separation of CSF, and gray and white matter for the whole brain. The presented segmentation method improves $\kappa = 0.913$ for the distorted and noisy phantom to $\kappa = 0.962$. A recently published value of $\kappa = 0.95$ achieved by the SPM method (Ashburner and Friston, 2000) indicates this to be a good quality. This is also exemplified by Fig. 1, in which the segmentation result for an axial and a sagittal slice is compared with the corresponding phantom tissues.

2.5. Analysis of geometry

The brain extraction was manually corrected if needed and the cerebellum as well as subcortical gray matter (basal ganglia, thalamus, preserving the hippocampus–amygdalar formation) were manually removed prior to segmentation. Applying the resulting maps on the segmented images yielded 3D maps of the cortical gray matter (GM) voxels of unitary brightness. The shape function of these images were Fourier-transformed with a routine for fast Fourier transform resulting in function $f(\mathbf{k})$, Eq. (3). The integration in Eq. (3) was performed numerically by subdividing k space in a number of spherical shells with logarithmically spaced thickness and computing the average k and $F(k)$ in each shell. The fractal dimension was found by fitting a linear function to the dependence of lg F on lg k. All computations were performed with in-house C programs.

3. Results

The main steps of the segmentation procedure are illustrated in Fig. 2 by showing representative T1-weighted images images of a segmented brain, and of the extracted supratentorial cortical gray matter, which was subjected to the geometry analysis.

Plots of the function $F(k)$ are shown in Fig. 3. The presence of an initial segment, which can be approximated by a straight line, suggests that the cortex is self-similar up to a region around $k = 1\ \mathrm{mm}^{-1}$. The corresponding length defined as π/k is 3 mm. The fractal dimensions in this range were found by fitting a linear function to the data points from the 1st to the 41st (which corresponds to $k = 1.0$

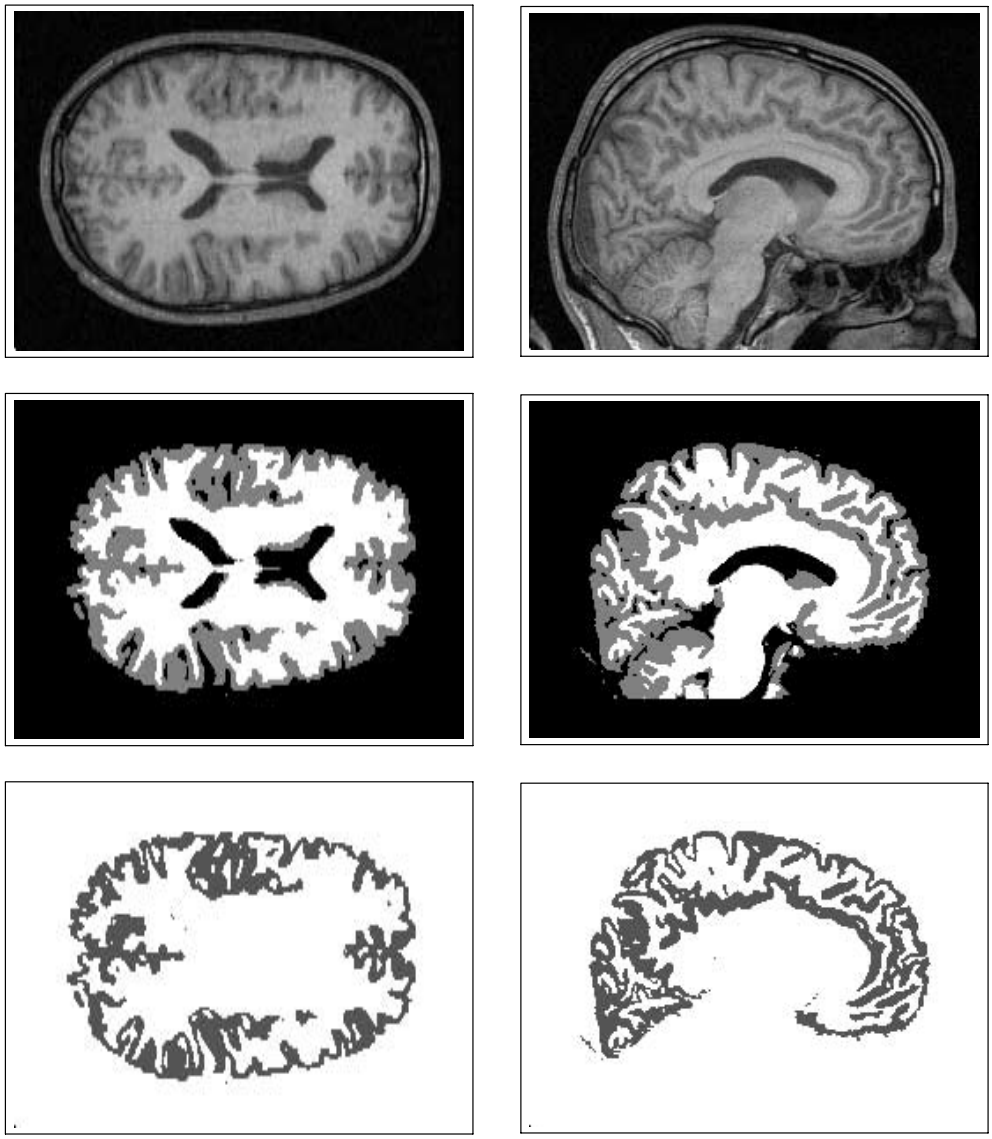

Fig. 2. An axial and a sagittal slice in one volunteer. Top panels: T1-weighted images. Middle panels: Results of the segmentation procedure. Bottom panels: Extracted cortical gray matter.

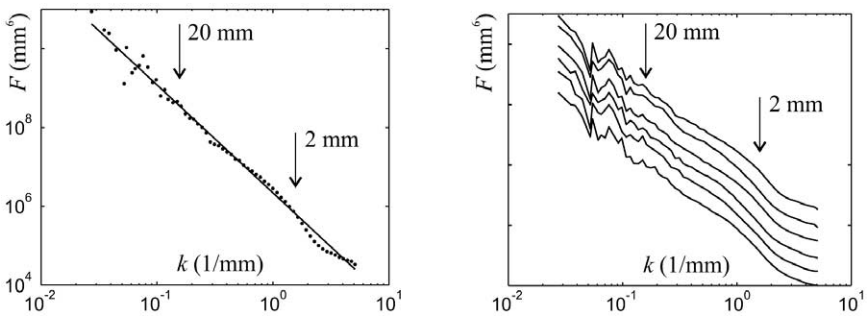

Fig. 3. Function $F(k)$ plotted vs k in double logarithmic scale. Left: Data for Subject 1. The straight lines show the result of an equal-weight fitting of function $\lg F(k) = Const - D\ 1g\ k$ to the data for the points through 1st to 41th. This results in the fractal dimension $D = 2.74 \pm 0.05$ shown in Table 1. The arrows indicate the values of k which correspond to given structure sizes in real space defined as π/k. The errors in the data are discussed in the text. Right: Similarly presented data for all six subjects with artificial shifts in the vertical direction.

Table 1
Fractal dimensions, *D*, found in all subjects for two length intervals

Subject	D (115–3.1 mm)	R	*D* (31–3.1 mm)	R
1	2.74±0.05	0.99977	2.76±0.04	0.99994
2	2.85±0.05	0.99980	2.62±0.04	0.99992
3	2.78±0.05	0.99979	2.65±0.03	0.99996
4	2.83±0.04	0.99985	2.75±0.04	0.99994
5	2.84±0.05	0.99978	2.76±0.03	0.99995
6	2.76±0.05	0.99983	2.62±0.03	0.99995
mean	2.80±0.05±0.02		2.69±0.07±0.01	

Note. The error (shown at one standard deviation) and the correlation coefficient, R, reflect the quality of fitting. The first error in the mean values is the standard deviation of the group averaging. The second error results from the fitting uncertainty for individual subjects.

mm^{-1}, Fig. 3). The results for all six subjects investigated are collected in Table 1. The group mean value is $D = 2.80 \pm 0.05 \pm 0.02$, where the first error defined at one standard deviation describes the interindividual variability and the second results from the fitting errors for individual subjects. The actual accuracy of the calculated fractal dimension is smaller due to the ambiguity in the interval in which the fitting is performed. For example, an application of the fitting to the data points from the 13th to the 41st (Fig. 3), which correspond to the length interval 31–3.1 mm, results in the group mean $D = 2.69 \pm 0.07 \pm 0.01$. Exclusion of the pathologic brain (Subject 6) does not result in any significant change in the mean fractal dimensions: $D = 2.81 \pm 0.05 \pm 0.02$ and $D = 2.71 \pm 0.07 \pm 0.01$ for the two above defined length intervals, respectively.

4. Discussion

The main result of the performed study is that the human cerebral cortex does show a nearly fractal geometry down to the spatial scale of 3 mm. This limit corresponds reasonably well to the cortical thickness. At larger *k* a finer spatial scale is probed at which the cortex is not subjected to folding.

The coarse spatial scale (small *k* in Fig. 3) is described with poor statistics. This follows from small numbers of grid points in Fourier space, which are averaged by computing individual *F* values (Fig. 4). One could expect that the shape of the $F(k)$ curve in this range is determined by the overall cortex structure, which is not subjected to statistical averaging involved in the definition of the fractal dimension. In contrast to these expectations, the self-similarity of the cortex folding sets up already for the largest spatial scales as suggested by the averaged linear behavior seen in Fig. 3 for the smallest *k*.

The present study shows the method's feasibility and reports first results for five healthy subjects and a focally abnormal brain. It is beyond the scope of this methodologic article to report a systematic analysis of cortical pathologies.

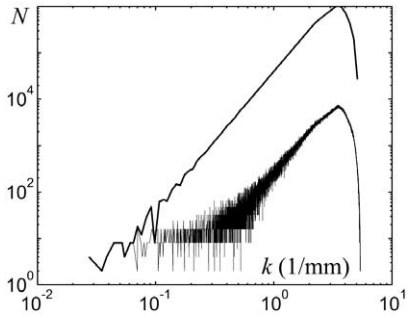

Fig. 4. Number of data points involved in the averaging over the directions of vector **k** in computing $F(k)$. The upper line is obtained for 61 intervals presented in Fig.3. The lower line shows the same value for 5409 intervals. $F(k)$ for this case is presented in Fig. 7. The coinciding initial parts of both lines are determined by a few grid points near the origin of *k* space. The slope of their main parts shows the dependence $N \propto k^3$. To explain this exponent, note that each *k* interval represents a thin spherical shell of radius *k* selected in three-dimensional *k* space. The shell surface increases quadratically, and its thickness is proportional to *k* for the used logarithmic spacing. The drop at large *k* is due to the rectangular shape of sampled *k* space.

4.1. Comparison with spherical geometry

Let us compare the function $F(k)$ characterizing the cortical geometry with that for a sphere of radius *R*. The latter can be obtained by a straightforward analytic calculation of the Fourier integral for the shape function, which equals unity inside and zero outside the sphere. Taking the squared magnitude results in

$$F(k) = \left(\frac{4\pi R}{k^2}\right)^2 \left(\cos kR - \frac{\sin kR}{kR}\right)^2. \quad (4)$$

We selected $R = 85$ mm in order to match the peculiarities seen for low *k* data points in Fig. 3. This value reasonably matches the brain size. Both dependencies are shown in Fig. 5. Although similar for the initial few points, the curves significantly differ from each other. First, the overall slope set by the first factor in Eq. (4) is equal to -4. Second, the oscillating factor in Eq. (4) results in many dips, which are

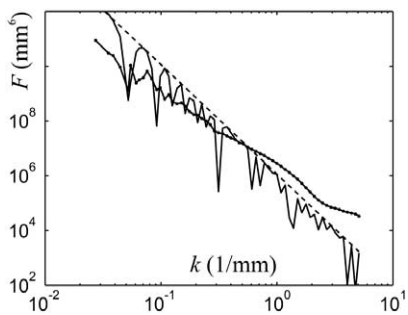

Fig. 5. A comparison of $F(k)$ for the cortex (the same data as shown in the left Fig. 3 with $F(k)$ calculated for a sphere of radius 85 mm, Eq. (4) (the irregular line). The dashed line shows the first nonoscillating factor in Eq. (4).

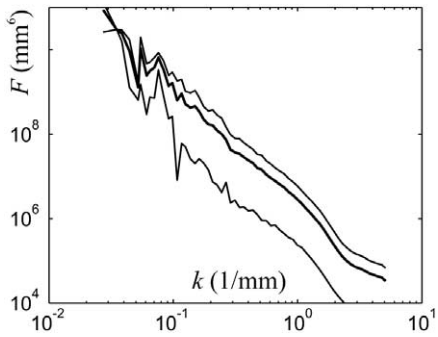

Fig. 6. Apparent errors in data shown in Fig. 3. The middle line reproduces function $F(k)$ for Subject 1 (Fig. 3 left). The error corridor is formed by the standard deviation, σ, of data averaged to obtain the values attributed to each k interval. Its magnitude is typically close to that of $F(k)$ and it marginally depends on k. The upper line shows $F(k) + \sigma(k)$. The lower line presents $F(k)e^{-\sigma(k)/F(k)}$. The latter formula coincides with $F(k) - \sigma(k)$ for small $\sigma(k)$ and helps avoiding negative values in the logarithmic scale. A deterministic origin of this seemingly large error is discussed in the text.

asymmetric in logarithmic scale. The apparently irregular shape of $F(k)$ for the sphere is due to an insufficient sampling of an oscillating line. The number of periods of the second factor in Eq. (4) is close to 14 for $k = 1\ \text{mm}^{-1}$. This comparison suggests that the peculiarities seen in the left Fig. 3 at small k do not originate from any noise. Rather they can be attributed to the overall brain shape. The same conclusion is suggested by the similarity of $F(k)$ for all subjects seen in Fig. 3.

4.2. More details about data averaging

The coarse brain structure clarifies the origin of the apparently large error in the data presented in Fig. 3. Fig. 6 shows the error corridor for the data presented in the left Fig. 3. The error bars were obtained as the standard deviation σ of the F values upon averaging in each k interval. The nearly constant $\sigma(k)$ rules out a purely random origin. Indeed, the number of averaged voxels enormously increases for large k as shown in Fig. 4. The conventional averaging of randomized deviations would result in a fast decreasing $\sigma(k)$. Why this is not the case can be explained by the following reasons. Consider an idealized cortex having an overall shape of an ellipsoid and the folding of which is similar in any direction from its center. Consider the function $|f(\mathbf{k})|^2$ of Eq. (3), which results in $F(k)$ after averaging over the direction of vector $\mathbf{k}$. The dependence $|f(\mathbf{k})|^2$ plotted against k would show a fractal dimension, which would be the same for all directions of vector $\mathbf{k}$. At the same time, the magnitude of $|f(\mathbf{k})|^2$ would be different in different directions according to the ellipsoid shape. The $F(k)$ values are obtained by the angular averaging in Eq. (3). In the considered example, this would be an averaging of many parallel lines with a significant spreading in their offsets. It would result in a constant $\sigma(k)$ similar to one presented in Fig. 6. For the ellipsoid, this effect could be corrected by an appropriate rescaling of, e.g., k_x and k_y. For real cortex, this is difficult due to its more complicated structure even at the coarser spatial scales.

The above reasoning is supported by data presented in Fig. 7 showing the effect of a finer k-gridding by computing the function $F(k)$. Treatment of $F(k)$ with less k intervals leads to more averaged values in each of them, while the smaller intervals present more individual contributions. Practically an apparently smooth $F(k)$ emerges when the number of averaged data points reaches one hundred, as it is seen from comparison of Fig. 7 and 4. The averaging, which is not performed in the fine k intervals, is effectively done later by fitting applied for computing the fractal dimension. It is possible to calculate more averaged $F(k)$ or let the averaging be achieved by fitting. These ways are not equivalent though. The former methods works with $F(k)$, thus complying with the definition of fractal dimension, while in the latter the effectively averaged quantity is $\lg F(k)$. The averaging of logarithm should yield a smaller dimension, which is the case shown in Fig. 7.

4.3. Summary of result uncertainties

The notion of fractal dimension is applicable to definite scale intervals, which should be given along with the final results. Obviously, intersubject comparison is meaningful only if equal intervals are applied. There may be several ways to equalize them. The simplest would be to always select equal k intervals. This is however less meaningful for cortices with a significant difference in size. A better way would be to appropriately rescale the considered k interval. Note that an image scaling does not change its fractal dimension up to the obvious restriction of the finite sampling. This uncertainty produces an error of a few percent, which is comparable with the accuracy of fitting.

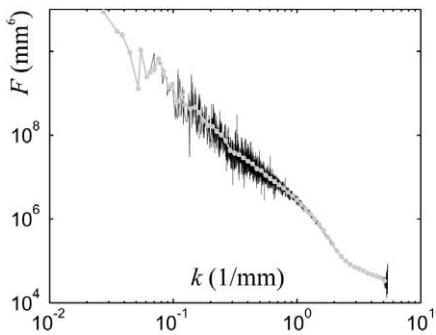

Fig. 7. Effect of reducing the k intervals in computing $F(k)$. The gray line with dots presents the same data as in the left Fig. 3. The less regular black line shows $F(k)$ for a subdivision of k axis in 5409 intervals. The number of data points in each interval is shown in Fig. 4. The fractal dimension found for the finely gridded data for the same k interval as in Fig. 3 is $D = 2.52 \pm 0.008$ (R = 0.99977). This is smaller than $D = 2.74 \pm 0.05$ obtained for the coarse gridding (Fig. 3, left, and Table 1), as should be expected by mathematical reasons discussed in the text.

Another uncertainty stems from the above-discussed way of averaging, which yields the $F(k)$ curve (Fig. 7). As is shown by the considered example, the fractal dimension can change by up to 10% for the extreme case presented in Fig. 7. The way of averaging should obviously be the same to enable intersubject comparison.

The results are also affected by the quality of segmentation. The ultimate accuracy of segmentation is limited by the presence of voxels containing tissue interfaces (the partial volume effect). Changing the segmentation thresholds might reassign such voxels to other tissue. In order to assess this effect, a segmentation threshold, which was used in assigning a voxel to either gray or white matter, was varied to produce once a 12% decrease and once an 11% increase in the number of gray matter voxels found in Subject 1. The corresponding variation in the fractal dimension in the interval 115–3.1 mm was nearly linear with the coefficient 0.006 per one percent change in the gray matter volume. As is seen from the data for individual subjects shown in Table 1, the fractal dimension remains within its error bar as long as the gray matter volume changes by less than 7–8%.

4.4. Comparison with other methods

Let us discuss how the present method relates to known approaches to characterize the cortical folding. Hofman (1991) has observed that the convoluted brains of terrestrial mammals possess an overproportional increase in the total cortical surface as a function of the brain volume, which is an indication of the fractal geometry. This areametric approach was further developed to the currently available methods (Majumdar and Prasad, 1988; Chuang et al., 1991; Cook et al., 1995; Free et al., 1996; Thompson et al., 1996). Appropriate computational methods imply counting the smoothed cortical area as a function of the smoothing extent. The smoothing hides fine details, thus providing a probe for different spatial scales. The difference between the known methods can be formulated in terms of the specific realization of measuring and smoothing the cortical surface. For example, Free et al. (1996) applied a dilation of the gray–white matter interface. This approach suffers from the abuttal of gyri, which explains its application to only the inner cortical surface (Free et al., 1996). The most precise surface reconstruction performed by Cook et al. (1995), Free et al. (1996), and Thompson et al. (1996) requires intensive computations, thus yielding a restricted amount of points for fitting the fractal dimension (from five to seven in the cited articles). The good fit quality obtained in these studies does not show this restriction as a disadvantage. However, it does not allow us to probe the cortical geometry over all scales.

In contrast, the present method is based on a volumetric approach. It avoids the problem of defining the interface areas in discretized three-dimensional images. The high computational efficiency allows for visualizing the gray matter geometry over all scales as shown, for example, in Fig. 3.

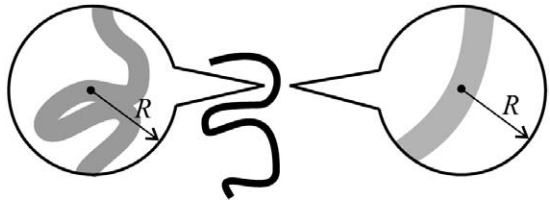

Fig. 8. An illustration of the smoothing of a convolved surface. The extent of smoothing is set by a sphere of radius R, which is shown before (left) and after the smoothing (right). Inside this sphere the convolved surface is replaced with a piece of a flat one (transition from left to right in the figure). At larger scales the overall surface shape is preserved (figure in the middle). The black dots represent a cortex element put in the origin of the sphere.

The price for these advantages is an incomplete comparability of the results derived from either areametric or volumetric calculations of the fractal dimension. Basically, both methods should yield similar results. Consider, for example, an idealized situation of the cortex with a constant thickness. Smoothing implies that the convolved cortex is replaced by a flat slightly curved surface at fine spatial scale up to some size R (Fig. 8). The surface structure at coarser scales is preserved. The original surface area $a(0)$ inside the smoothing sphere can be estimated as the volume inside this sphere divided by the cortex thickness Δ. This is $a(0) \propto R^D/\Delta$ according to the definition of the fractal dimension. This area is replaced upon smoothing by $a(R) \propto R^2/\Delta$, which corresponds to an unfolded surface. Thus the surface area inside the smoothing sphere is reduced by a factor $a(R)/a(0) \propto R^{2-D}$. As this estimate is applicable to each cortex element, the same relation holds for the whole smoothed surface area. This is the formula used in previous studies to measure the fractal dimension in three dimensions (Chuang et al., 1991; Free et al., 1996; Thompson et al., 1996).

This example supports the idea that the areametric and the volumetric approaches should yield similar results for the fractal dimension. How close the results would be is however difficult to predict. First, the cortical thickness is not constant. Second, any practical realization of the areametric approach needs to specify the means of smoothing. The implementation by Free et al. (1996) involves nonanalytical operations such as thresholding, which hinders a precise analytical analysis. Third, the available in vivo areametric results are obtained for either inner or outer cortical surface, while the present method works with the whole cortical volume. Against this background, one may expect numerically small, but systematic differences between the fractal dimensions derived from the two methods and from different realizations of the areametric approach.

This is supported by the available results. The fractal dimension found by Free et al. (1996) for the inner cortical surface is 2.30 ± 0.01. Extrapolation of the planar fractal dimension 1.45 ± 0.06 obtained by Cook et al. (1995) from

two to three dimensions would give $D = 2.45$. Blanton et al. (2001) presented graphical results centered near $D = 2.26$. These values are reasonably smaller than the volumetric one found in the present study. One can expect that the volumetric result is closer to the outer cortical area, as the latter is larger. The fractal dimension of this interface was found to be 2.60 ± 0.05 (Majumdar and Prasad, 1988). The deviation from the presented result $D = 2.80 \pm 0.05$ can be accepted in view of the above-discussed systematic difference in the computation methods.

An alternative established measure of the cortical folding is the gyrification index (GI) (Zilles et al., 1988). It is based on length measurements in brain sections. The gyrification index for a section is the ratio of the total length of the dissected cortical area to the length of outer contour around the section. The mean GI for a hemisphere is defined as the ratio of sum over sections of all total lengths to the sum of all outer contour lengths.

The notions of both the fractal dimension and the GI rely on a comparison between the overall size of the brain and the size of the folded cortex. The similarity ends here though. Calculations of GI make use of the extreme of the largest scale (the outer contour) and of the finest scale, at which the total cortical section length is measured. Since the outer contour cannot be treated statistically, it is difficult to deduce a mathematical relation between the GI and the cortical fractal dimension. It would be in the spirit of fractal calculus to consider the contours, which are smoothed to different extent. In practice, the GI focuses on rather location-specific information without referring to variable spatial scales. Both measures may provide complementary information which may be useful for characterizing abnormal cortical folding. The fractal dimension over all spatial scales in the presented structurally malformed brain was unremarkable despite a clearly abnormal focal cortical thickening. This is in line with only about half of the patients with structural abnormalities studied by Free et al. (1996) showing abnormal fractal dimensions. On the other hand, fractal analysis may be adapted to detect locally restricted abnormalities when applied to regions of interest. The advantage of the whole cortical analysis to study brain diseases can be mainly seen in assessing subtle global changes in folding structure which may be associated with abnormal brain development and neurodegeneration.

5. Summary

An analysis of the geometry of the human cerebral cortex has been performed over all spatial scales. It was shown that the cortex does possess a self-similarity extending to details of about 3 mm. The fractal dimension in this range agrees reasonably well with previously reported values. The new calculational method is based on the fast Fourier transform of segmented three-dimensional high-resolved magnetic resonance images. The resulting computational algorithm is extremely effective and involves only standard methods of classical mathematics, making this approach well suited to further neuroimaging studies focusing on cerebral shape abnormalities.

Acknowledgments

One of us (V.G.K.) acknowledges the kind help of D. Gembris, S. Wiese, M. Zaitsev and a useful discussion with K. Zilles. We thank K. Rodenacker for important contributions to the segmentation procedure. This work was supported in part by DFG SFB386.

Appendix

Equivalence of direct and Fourier determination of fractal dimension

The presented proof is a modification of one given by Liu (1986) for the context of brain MRI.

The cortex is described by the shape function, $s(\mathbf{r})$, introduced in Section 2.2, which is unity in the cortical gray matter and zero otherwise. The Fourier transform of this function, $f(\mathbf{k})$, in Eq. (3), has the following explicit form:

$$f(\mathbf{k}) = \int_{-\infty}^{\infty} dx \int_{-\infty}^{\infty} dy \int_{-\infty}^{\infty} dz s(\mathbf{r}) e^{\mathbf{ikr}} \equiv \int s(r) e^{\mathbf{ikr}} d^3\mathbf{r}. \quad (5)$$

Here x, y, and z are the components of vector $\mathbf{r}$. The second integral form introduces a short-hand notation, which is useful for writing the following multidimensional integrals. In this notation only the integration measure is given explicitly. $F(k)$ defined in Eq. (3) takes the form

$$F(k) = \frac{1}{4\pi} \int_0^{2\pi} d\varphi \int_0^{\pi} d\theta \sin\theta\, f(\mathbf{k})\, f^*(\mathbf{k}) \equiv \int f(\mathbf{k})\, f^*(\mathbf{k}) \frac{d\Omega_k}{4\pi}, = \int s(\mathbf{r}) s(r') e^{-\mathbf{ik}(\mathbf{r}-\mathbf{r}')}\, d^3\mathbf{r} d^3\mathbf{r}' \frac{d\Omega_k}{4\pi}. \quad (6)$$

Here φ and θ, which have been introduced in Eq. (3), define the direction of $\mathbf{k}$. The second integral in the first line introduces a short-hand notation for the integration over

these two angles. Let us change the integration variable from $\mathbf{r}$ to $\Delta\mathbf{r} = \mathbf{r} - \mathbf{r}'$ and integrate then over $\mathbf{r}'$. This gives

$$F(k) = \int s(\mathbf{r}' + \Delta\mathbf{r})s(\mathbf{r}')e^{-i\mathbf{k}\Delta\mathbf{r}}d^3\Delta\mathbf{r}d^3\mathbf{r}'\frac{d\Omega_k}{4\pi}$$

$$= \int \rho(\Delta\mathbf{r})e^{-i\mathbf{k}\Delta\mathbf{r}}d^3\Delta\mathbf{r}\frac{d\Omega_k}{4\pi}, \quad (7)$$

where $\rho(\Delta\mathbf{r})$ is the two-point correlation function of the cortex for the given spacing $\Delta\mathbf{r}$. Now we use the property of the Fourier transform that a rotation in the source results in the opposite rotation of the image. To do it accurately, let us define a fixed vector $\mathbf{k}_0$ and obtain all directions of the integration variable $\mathbf{k}$ as $\mathbf{k} = O\mathbf{k}_0$, where O is a rotation matrix. This results in the following form of F(k),

$$F(k) = \int \rho(\Delta\mathbf{r})e^{-i\mathbf{k}0O^{-1}\Delta\mathbf{r}}d^3\,\Delta\mathbf{r}\frac{d\Omega_k}{4\pi}$$

$$= \int \rho(O\Delta\mathbf{r}')e^{-i\mathbf{k}_0\Delta r'}d^3\,\Delta\mathbf{r}'\frac{d\Omega_k}{4\pi}, \quad (8)$$

where we have changed the integration variable $\Delta\mathbf{r}$ to $\Delta\mathbf{r}' = O^{-1}\,\Delta\mathbf{r}$ and used the property $O^{\mathrm{t}} = O^{-1}$. Note that Ω_{k} still defines the rotation angles of the matrix O. Thus the integration over Ω_{k} performs the averaging of $\rho(O\Delta\mathbf{r}')$ over the orientations of its argument. This gives the definition of the fractal dimension D:

$$\int \rho(\Delta r)\frac{d\Omega_k}{4\pi} \propto (\Delta r)^{D-3}. \quad (9)$$

Substituting this into Eq. (8) and calculating the Fourier integral we finally obtain that

$$F(k) \propto k^{-D} \quad (10)$$

if D does not depend on $\Delta\mathbf{r}$.

References

Ashburner, J., Friston, K., 2000. Voxel-based morphometry—the methods. NeuroImage 11, 805–821.

Blanton, R., Levitt, J., Thompson, P., Narr, K., Capetillo-Cunliffe, L., Nobel, A., Singerman, J., McCracken, J., Toga, A., 2001. Mapping cortical asymetry and complexity patterns in normal children. Psychiatr. Res. Neuroimaging Sect. 107, 29–43.

Chuang, K., Valentino, D., Huang, H., 1991. Measuring the fractal dimension using 3D technique. Proc. SPIE Image Process 1445, 341–347.

Cocosco, C., Kollokian, V., Kwan, K., et al., 1997. Brainweb: online interface to a 3D MRI simulated brain database. NeuroImage 5, 425.

Cook, M., Free, S., Manford, M., Fish, D., Shorvon, S., Stevens, J., 1995. Fractal description of cerebral cortical pattens in frontal lobe epilepcy. Eur. Neurol. 35, 327–335.

Dale, A., Fischl, B., Sereno, M., 1999. Cortical surface-based analysis. NeuroImage 9, 179–194.

Free, S., Sisodiya, S., Cook, M., Fish, D., Shorvon, S., 1996. Three-dimensional fractal analysis of the white matter surface from magnetic resonance images of the human brain. Cerebral Cortex 6, 830.

Hahn, K., Rodenacker, K., Auer, D., 2000. Segmentierung des Gehirns auf der Basis von MR-Daten, in: BVM 2000, Springer, pp. 86–90.

Hahn, K., Rodenacker, K., Auer, D., 2001a. Cortex homogenization for intensity segmentation—an alternative. NeuroImage 13 (6), 141.

Hahn, K., Rodenacker, K., Kempe, A., et al., 2001b. Intensitätssegmentierung von T1-gewichteten MR Gehirndaten über die Homogenisierung der grauen oder der weiBen Materie—eine vergleichende Studie, in: BVM 2001, Springer, pp. 207–211.

Hofman, M., 1991. The fractal geometry of convoluted brains. J. Hirnforschung 32, 103.

Kwan, K., Evans, A., Pike, G., 1996. An extensible MRI simulator for post-processing evaluation, in, Proc. Conference on Visualistion in Biomedical Computing, pp. 135–140.

Liu, S., 1986. Fractals and their Applications in Condensed Matter Physics. Academic Press, New York.

Majumdar, S., Prasad, R., 1988. The fractal dimension of cerebral surfaces using magnetic resonance imaging. Comput. Phys. Nov/Dec, 69–73.

Thompson, P., Schwartz, C., Lin, R., Khan, A., Toga, W., 1996. Three-dimensional statistical analysis of sulcal variability in the human brain. J. Neurosci. 16, 4261–4274.

Zilles, K., Amstrong, E., Schleicher, A., Kretschmann, H., 1988. The human pattern of gyrification in the cerebral cortex. Anat. Embriol. 179, 173–179.